

Online Research @ Cardiff

This is an Open Access document downloaded from ORCA, Cardiff University's institutional repository: <https://orca.cardiff.ac.uk/133779/>

This is the author's version of a work that was submitted to / accepted for publication.

Citation for final published version:

Li, Zhibo, Allford, Craig P., Shutts, Samuel, Forrest, Adam F., Alharbi, Reem, Krysa, Andrey B., Cataluna, Maria Ana and Smowton, Peter M. 2020. Monolithic InP quantum dot mode-locked lasers emitting at 730 nm. IEEE Photonics Technology Letters 32 (17) , pp. 1073-1076. file

Publishers page: <http://dx.doi.org/10.1109/LPT.2020.3012568>
<<http://dx.doi.org/10.1109/LPT.2020.3012568>>

Please note:

Changes made as a result of publishing processes such as copy-editing, formatting and page numbers may not be reflected in this version. For the definitive version of this publication, please refer to the published source. You are advised to consult the publisher's version if you wish to cite this paper.

This version is being made available in accordance with publisher policies.

See

<http://orca.cf.ac.uk/policies.html> for usage policies. Copyright and moral rights for publications made available in ORCA are retained by the copyright holders.



Monolithic InP Quantum Dot Mode-Locked Lasers Emitting at 730 nm

Zhibo Li, Craig P. Allford, Samuel Shutts, Adam F. Forrest, Reem Alharbi, Andrey B. Krysa, Maria Ana Cataluna and Peter M. Smowton

Abstract—This letter reports on InP/GaInP quantum dot mode-locked lasers emitting in the 730 nm wavelength region, extending the spectral range of previously reported monolithic mode-locked edge-emitting lasers. Modal gain and absorption measurements were used to identify a relatively broad spectrum which is utilised to support passive mode-locking in a monolithically integrated two-section ridge laser. The conditions for mode-locking were explored by varying the current to the gain section and reverse bias to the absorber section. For a total cavity length of 3 mm, the shortest pulse train observed was 6 ps in duration with a repetition rate of 12.55 GHz.

Index terms—mode-locked laser diode, monolithic integration, InP quantum dots

I. INTRODUCTION

SEMICONDUCTOR quantum-dots (QDs) materials have demonstrated great promise for ultrashort optical pulse generation and amplification, owing to their broad optical gain/absorption spectra, resulting from their inhomogeneous dot size distribution, as well as fast carrier dynamics. Previous work on electrically pumped QD mode-locked lasers (MLLs) has focused primarily on InAs QDs emitting in the infrared spectral region, targeting the C- or O-bands [1]–[3]. On the other hand, InP/GaInP QDs materials have allowed to successfully access the visible range in the red spectral region, driven by pulsed current sources [4]–[8]. InP/GaInP QD materials have also shown ultrafast absorption recovery times, which has allowed their use as semiconductor saturable absorber mirrors, for example, to mode-lock Ti: Sapphire lasers [9]. In addition, the gain recovery time for InP QDs has been shown to be even faster than for InAs QDs, dominated by a sub-200 fs component [10]. The potential for ultrafast electrically-pumped monolithic mode-locked QD lasers operating at visible wavelengths where there are numerous applications requiring short optical pulses have yet to be

Manuscript submitted June 03, 2020; revised July 05, 2020. This work was support by the UK Engineering Physical Sciences Research Council (EPSRC) under grant number EP/P006973/1 and EP/P030556/1. A. F. Forrest and M. A. Cataluna acknowledge funding by the European Research Council (ERC) under the European Union’s Horizon 2020 research and innovation programme (grant agreement No 640537).

Z. Li, C. P. Allford, S. Shutts, R. Alharbi and P. S. Smowton are with School of Physics & Astronomy, Cardiff University, Cardiff, CF24 3AA, UK (liz74@cardiff.ac.uk; allfordcp1@cardiff.ac.uk; shutts@cardiff.ac.uk; alharbirs@cardiff.ac.uk; smowtonpm@cardiff.ac.uk).

A. F. Forrest and M. A. Cataluna are with School of Engineering and Physical Sciences, Heriot-Watt University, Edinburgh, EH14 4AS, UK (adam.forrest@hw.ac.uk; m.cataluna@hw.ac.uk).

A. B. Krysa is with Department of Electronic and Electrical Engineering, University of Sheffield, Sheffield, S1 3JD, UK (a.krysa@sheffield.ac.uk).

R. Alharbi is with Physics Department, King Abdulaziz University, Jeddah, Saudi Arabia.

The data underpinning the results presented in this paper can be found in the Cardiff University data catalogue with the Digital Object Identifier 10.17035/d.2020.0111414926.

exploited. These include high-resolution biomedical fluorescence imaging, targeted cell transfection and biological nanosurgery, all of which would benefit from more compact and lower-cost optical sources [11]–[13]. To date, the shortest wavelengths in the red side of the visible spectrum accessed by monolithic electrically-pumped MLLs were 760 nm and 752 nm [14], [15], using AlGaAs multi-quantum-well structures.

Here we report broad optical gain and absorption spectra for InP/GaInP QDs and demonstrate passive mode-locking in monolithic integrated two-section lasers using this material, enabling the first demonstration of ultrashort pulse generation from electrically-pumped QD lasers around 730 nm. Subsequently, this is the shortest wavelength on the red side of the visible spectrum to ever be accessed by a monolithic integrated passive mode-locked edge-emitting laser.

II. DEVICE STRUCTURE AND FABRICATION

The laser structure, as shown in Fig. 1(a), was grown by metal-organic chemical vapour deposition (MOCVD) on n-GaAs (100) substrates oriented 10° off toward $\langle 111 \rangle_A$, using trimethyl precursors for the group III elements and AsH₃ and PH₃ as precursors of the group V elements. The active region consisted of five dots-in-well (DWELL) layers, where each layer of dots was formed from 7.5 Å of InP self-assembled QDs on an (Al_{0.3}Ga_{0.7})_{0.51}In_{0.49}P matrix and then covered with a 8 nm Ga_{0.51}In_{0.49}P quantum well. Separate samples grown with a similar recipe were found to have a dot density of 10^{10} cm⁻² [16]. A 16 nm (Al_{0.3}Ga_{0.7})_{0.51}In_{0.49}P barrier separated each DWELL layer. The remainder of the waveguide was formed by 100 nm un-doped (Al_{0.3}Ga_{0.7})_{0.51}In_{0.49}P separate confinement heterostructure (SCH) layers and 1000 nm Al_{0.51}In_{0.49}P cladding layers, doped with Si and Zn for n- and p-types, respectively. Finally, a 300 nm highly p-doped cap-layer of GaAs was deposited as the top contact.

The MLLs were fabricated by firstly patterning 2 μm wide shallow-etched ridge-waveguides by electron beam lithography and dry-etching using a chlorine-based inductively coupled plasma (ICP) process which was stopped just above the active region. A gap between the gain section and saturable absorber (SA) was defined with a width of 20 μm, with the top contact p-GaAs layer in the gap removed to achieve sufficient electrical isolation. The ridges were then planarized by spin-coating benzocyclobutene (BCB), followed with a back-etch process utilizing fluorine-based reactive ion etching until the ridge top was fully exposed. Cr/Au was then deposited as a p-contact metal and AuGe/Ni/Au was deposited on the substrate-side after lapping to 100 μm, to form the n-contact.

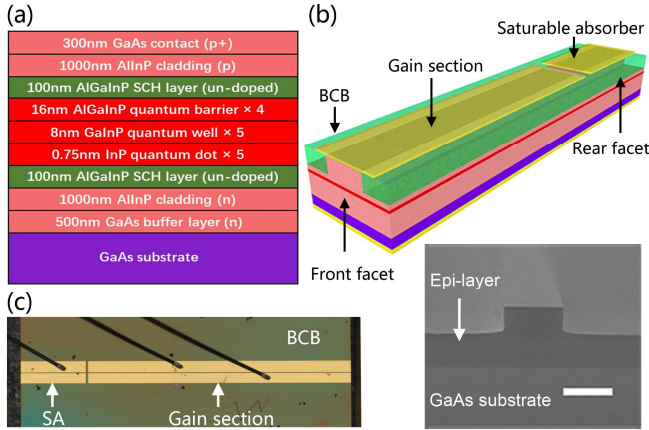


Fig. 1. (a) InP/GaNnP QD laser structure, (b) schematic of monolithic integrated two section passive MLL, with inset SEM image showing the cross-section profile of ridge cavity prior to the BCB planarization, the scale bar is 2 μm , (c) optical microscope image of a 3 mm long MLL.

Fig. 1(b) shows a diagram of a fabricated InP QD MLL, and a scanning electron microscope (SEM) image of the cross-section profile of the ridge before the BCB planarization. The epitaxial layers and the GaAs substrate can be easily distinguished, and the active region can be identified under the ridge. Finally, the fabricated chip was cleaved into laser bars, then mounted and wire-bonded on transistor-outline (TO) headers for measurements. MLLs were cleaved with a total cavity length of 3 mm comprising of a 2.4 mm gain section, 0.6 mm saturable absorber (SA) section and with uncoated as-cleaved facets. An optical microscope image of a completed MLL is shown in Fig. 1(c), where the bonding wires can be seen, with two wires bonded on each side of the ridge in the gain section for a uniform current supply. Non-lasing oxide-isolated stripe broad-area segmented contact devices, with 50 μm wide and 600 μm long contacts, were also fabricated to study the material’s optical properties.

III. RESULTS AND ANALYSIS

The segmented contact method was used to determine the material’s optical gain and absorption spectra by comparing the amplified spontaneous emission (ASE) from two contact sections with identical length [17]. The front two sections were driven by a pulsed current source, with 1.0 μs pulse length and 0.1% duty cycle to avoid self-heating. To eliminate round-trip amplification, the non-lasing test structures were fabricated with contact stripes orientated perpendicular to the 10° off-axis facet.

Fig. 2(a) shows the net modal gain and absorption spectra measured at room temperature. Increasing the injection current per section from 80 mA (0.27 kA/cm^2) to 150 mA (0.5 kA/cm^2) broadens the gain spectra bandwidth (full-width half-maximum - FWHM) from 14 nm to 29 nm. The internal optical loss, α_i , taken at wavelengths beyond the band-edge was found to be $\sim 6 \text{ cm}^{-1}$. The absorption curve shown in Fig. 2(a) (black dashed line) was determined by separately pumping (forward biasing) each of the front two sections of a segmented contact device in-turn and comparing the ASE, as described in [17]. The sections not being pumped are

grounded and therefore the resulting spectrum shown represents the modal absorption at 0V i.e. without reverse bias.

Fig. 2(b) plots the peak net modal gain values and the corresponded peak wavelength respective to the injection currents. The peak net modal gain of -1.55 cm^{-1} at 40 mA (0.13 kA/cm^2) is increased to 6.5 cm^{-1} at 150 mA (0.5 kA/cm^2), whereas the peak wavelength is blue-shifted from 726 nm to 713 nm. This is largely due to state-filling of inhomogeneous distributions of energy states associated with the ensemble of small and large dot sizes. Recombination from the excited dot states at shorter wavelengths starts to play a role at higher injection currents [18]. These broad gain and absorption spectra show the potential to support the generation of ultrashort pulses.

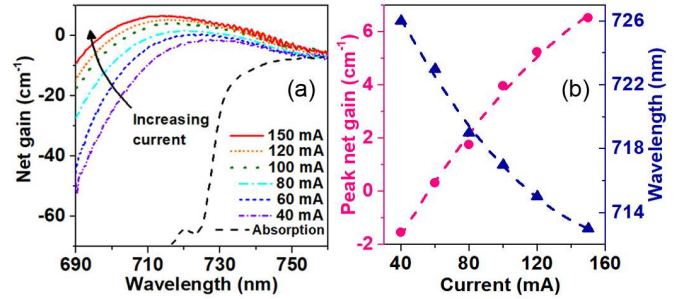


Fig. 2. Experimental results of (a) optical net modal gain and absorption of InP/GaNnP QD laser materials and plots of (b) peak net gain values (circles) and the corresponding gain spectra peak wavelength (triangles) under the corresponding injection current.

To measure the light-current (L-I) characteristics of the MLLs, the gain section was forward biased with continuous waveform (CW) current injection, whilst the SA section was driven with either a forward current injection, unbiased (floating), or under reverse bias conditions. The single-facet laser power was measured using an integrating sphere and all results were taken at a device heatsink temperature of 10°C unless otherwise stated. As can be seen from the results shown in Fig. 3, with the SA section forward biased, the MLL operates as Fabry-Perot (FP) laser with a threshold current of 14 mA, reaching an optical power of over 10 mW at 90 mA. When reverse bias was applied to the SA section, a reduction in power was observed, decreasing to 4.8 mW and 2 mW when the SA section was biased to -1 V and -3 V respectively, whilst maintaining a constant gain section current of 90 mA. Abrupt changes in the L-I characteristic can be observed above threshold due to the presence of and the transfer between multiple lateral modes [19]. However, when the reverse bias is increased beyond 2 V the L-I characteristics get smoother, which is likely due to the attenuation of the unwanted lateral modes by enhanced absorption.

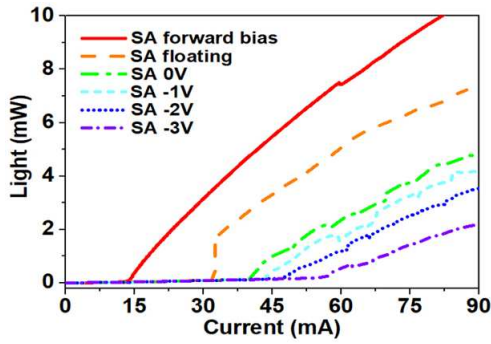


Fig. 3. L-I curves of a 3 mm long InP/GaInP MLL with the gain section forward biased and the SA under various bias conditions.

To characterise the mode-locking performance, the emission from the front facet (gain section) was first collimated then focused by a second lens to allow coupling into a 1×2 single-mode fibre splitter, with 80% and 20% output ports connected to a fast photodetector and an optical spectrum analyser, respectively. The fast photodetector was connected to an electrical spectrum analyser and a flip-mirror was implemented such that the beam could be either coupled into the fibre mentioned above or directed to the autocorrelator, operating in non-collinear mode. This setup allowed the repetition frequency, lasing spectrum and pulse width to be visualized at the same time, under identical bias conditions. An optical isolator and a half-wave plate were included to minimize feedback to the device and maintain the appropriate polarization direction.

The shortest pulse duration measured from a 3 mm cavity length MLL was achieved at a gain section drive current of 80 mA and 2.74 V SA reverse bias. The corresponding radio frequency (RF) electrical spectrum, autocorrelator signal and the lasing spectrum are shown in Fig. 4 (a) – (b), respectively. A repetition frequency of 12.55 GHz was obtained with the RF signal intensity over 50 dB as shown in Fig. 4 (a). The 3-dB bandwidth of the RF peak was 21 kHz, measured with a scanning span of 10 MHz and resolution bandwidth (RBW) of 1 kHz. The inset figure shows the RF signals from a wider scan range with the RBW of 100 kHz. A very strong second harmonic RF peak at 25.1 GHz is also clearly seen. Fig. 4 (b) shows the autocorrelation signal measured from the pulse (solid red) and its secant squared fit result (dashed blue). The pulse-width of 6 ps can be determined from the FWHM of the autocorrelation trace. The inset figure shows the measured lasing spectrum from the optical spectrum analyser, where the peak lasing wavelength is 734.69 nm and the FWHM is 0.18 nm. The average single-facet power, measured after the optical isolator, exceeded 1.74 mW and the corresponding peak power was over 23 mW.

Fig. 5 shows the evolution of the pulse-width with reverse bias where the gain current was fixed to 80 mA. The pink (triangles) data points indicate the pulse-width measured at each reverse bias and showing a decreasing trend from 15.6 ps at 1.06 V reverse bias down to 6 ps at 2.74 V. This is due to the reduction in the absorption recovery time which is induced by a faster carrier sweep-out time at higher reverse biases [20]. Time bandwidth products (TBP) of these pulses were also

calculated and plotted in Fig. 5 (circles), showing that all values are below 0.6, with the smallest of 0.35 approaching the theoretical transform-limit of 0.315, assuming a sech²-shaped pulse. This implies that although some chirp may exist due to the interplay of gain and absorption and self-phase modulations [21], these pulses still exhibit stable mode-locking behaviour.

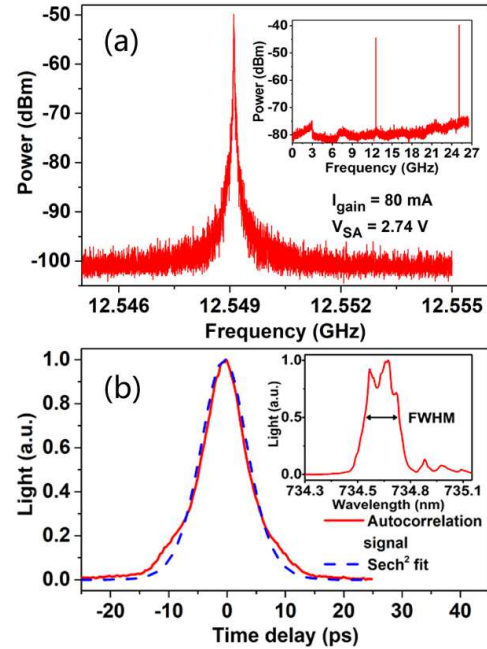


Fig. 4. Ultrafast pulse characterizations of a 3 mm long InP/GaInP MLL, (a) shows the RF spectrum indicating a repetition frequency of 12.55 GHz, (b) plots the experimental autocorrelation signal and fit (assuming a sech² pulse shape), resulting in a pulse-width of 6 ps, inset: lasing spectrum with a peak of 734.69 nm and FWHM of 0.18 nm.

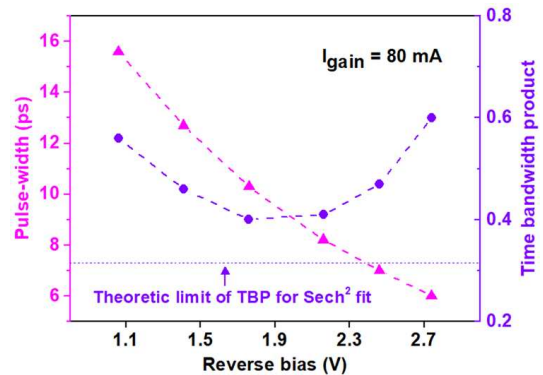


Fig. 5. Pulse-widths (triangles) measured at a reverse bias of 1.06 V, 1.41 V, 1.76 V, 2.16 V, 2.46 V and 2.74 V whereas the gain current was fixed to 80 mA, and the corresponding time bandwidth product values (circles).

To further investigate the influence of gain current on the mode-locking behaviour, a fixed reverse bias of 1.85 V was applied to the SA section whilst the gain current was increased gradually. Fig. 6 compares autocorrelation traces and the corresponding optical spectra measured with gain currents of 75 mA, 80 mA and 85 mA. A decrease in pulse-width from 20 ps to 8 ps was observed with increasing gain current. Simultaneously, the lasing wavelength was blue-shifted from

735.6 nm to 733.2 nm, which we attribute to the higher injection currents allowing the optical gain peak to shift to shorter wavelengths. This state-filling phenomenon also is in line with the gain measurement results shown in Fig. 2 and suggests the gain is not fully clamped over the QD ensemble under these lasing conditions.

While the measured pulse lengths approaches those predicted from the time-bandwidth product, we note that the broad optical gain spectrum of Fig. 2 is not being exploited effectively in these devices with a lasing spectrum width of only 0.18 nm (Fig. 4). We postulate that the limitation is the manner in which carriers are distributed across the dot states rather than dispersion or effects associated with the alpha factor. Therefore, while measured pulse lengths are appropriate for applications, we expect that further progress on shortening pulse width should be possible with significant improvement in the gain available from the quantum dots, the concomitant reduction in carrier density at threshold and improved carrier localisation.

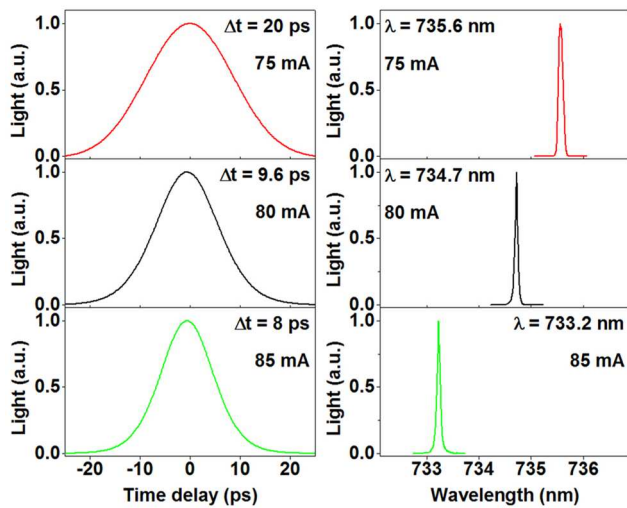


Fig. 6. Pulse-widths and optical spectra measured at 75 mA, 80 mA and 85 mA gain current, the reverse bias was fixed to 1.85 V.

IV. CONCLUSION

In summary, monolithic integrated passive MLLs emitting around 730 nm have been demonstrated. The shortest pulse generated from a MLL with a 3 mm cavity length was 6 ps with a 12.55 GHz repetition rate. This work demonstrates the potential of using this InP/GaInP QD materials to achieve low cost and compact MLLs as ultrafast light sources, opening up a new range of functionalities for MLLs by pushing the spectral boundaries into the visible region, which is highly relevant in biomedical imaging and cell biology applications.

REFERENCES

[1] E. U. Rafailov, M. A. Cataluna, and W. Sibbett, "Mode-locked quantum-dot lasers," *Nature Photonics*, Review Article vol. 1, p. 395, 07/01/online 2007.
 [2] P. Finch, et al., "Improving the Optical Bandwidth of Passively Mode-Locked InAs Quantum Dot Lasers," *IEEE Journal of Selected Topics in Quantum Electronics*, vol. 21, no. 6, pp. 674-680, 2015.

[3] M. G. Thompson, et al., "InGaAs Quantum-Dot Mode-Locked Laser Diodes," *IEEE Journal of Selected Topics in Quantum Electronics*, vol. 15, no. 3, pp. 661-672, 2009.
 [4] M. K. Zundel *et al.*, "Red-light-emitting injection laser based on InP/GaInP self-assembled quantum dots," *Applied Physics Letters*, vol. 73, no. 13, pp. 1784-1786, 1998.
 [5] G. Walter, N. H. Jr., J. H. Ryou, and R. D. Dupuis, "Coupled InP quantum-dot InGaP quantum well InP-InGaP-In(AlGa)P-InAlP heterostructure diode laser operation," *Applied Physics Letters*, vol. 79, no. 20, pp. 3215-3217, 2001.
 [6] S. Shutts, S. N. Elliott, P. M. Smowton, and A. B. Krysa, "Exploring the wavelength range of InP/AlGaInP QDs and application to dual-state lasing," *Semiconductor Science and Technology*, vol. 30, no. 4, p. 044002, 2015/03/05 2015.
 [7] P. M. Smowton, et al., "InP-GaInP quantum-dot lasers emitting between 690-750 nm," *IEEE Journal of Selected Topics in Quantum Electronics*, vol. 11, no. 5, pp. 1035-1040, 2005.
 [8] Z. Huang, M. Zimmer, S. Hepp, M. Jetter, and P. Michler, "Optical Gain and Lasing Properties of InP/AlGaInP Quantum-Dot Laser Diode Emitting at 660 nm," *IEEE Journal of Quantum Electronics*, vol. 55, no. 2, pp. 1-7, 2019.
 [9] V. G. Savitski *et al.*, "Passive Mode-Locking of a Ti : Sapphire Laser by InGaP Quantum-Dot Saturable Absorber," *IEEE Photonics Technology Letters*, vol. 22, no. 4, pp. 209-211, 2010.
 [10] W. Langbein, et al., "Ultrafast gain dynamics in InP quantum-dot optical amplifiers," *Applied Physics Letters*, vol. 97, no. 21, p. 211103, 2010.
 [11] M. Kuramoto, N. Kitajima, H. Guo, Y. Furushima, M. Ikeda, and H. Yokoyama, "Two-photon fluorescence bioimaging with an all-semiconductor laser picosecond pulse source," *Opt. Lett.*, vol. 32, no. 18, pp. 2726-2728, 2007/09/15 2007.
 [12] U. K. Tirlapur and K. König, "Targeted transfection by femtosecond laser," *Nature*, vol. 418, no. 6895, pp. 290-291, 2002/07/01 2002.
 [13] A. Vogel, J. Noack, G. Hüttman, and G. Paltauf, "Mechanisms of femtosecond laser nanosurgery of cells and tissues," *Applied Physics B*, vol. 81, no. 8, pp. 1015-1047, 2005/12/01 2005.
 [14] H. Wang *et al.*, "Ultrashort pulse generation by semiconductor mode-locked lasers at 760 nm," *Opt. Express*, vol. 22, no. 21, pp. 25940-25946, 2014/10/20 2014.
 [15] L. Kong *et al.*, "Deep-red semiconductor monolithic mode-locked lasers," *Applied Physics Letters*, vol. 105, no. 22, p. 221115, 2014.
 [16] M. S. Al-Ghamdi, P. M. Smowton, S. Shutts, P. Blood, R. Beanland, and A. B. Krysa, "Absorption, Gain, and Threshold in InP/AlGaInP Quantum Dot Laser Diodes," *IEEE Journal of Quantum Electronics*, vol. 49, no. 4, pp. 389-394, 2013.
 [17] P. Blood, et al., "Characterization of semiconductor laser gain media by the segmented contact method," *IEEE Journal of Selected Topics in Quantum Electronics*, vol. 9, no. 5, pp. 1275-1282, 2003.
 [18] S. Shutts, P. M. Smowton, and A. B. Krysa, "InP quantum dot lasers with temperature insensitive operating wavelength," *Applied Physics Letters*, vol. 103, no. 6, p. 061106, 2013.
 [19] J. W. R. t. Cate, L. M. Weegels, A. H. v. Bakel, C. J. v. d. Poel, and H. P. M. M. Ambrosius, "Kinks induced by free-carrier absorption in weakly index guided semiconductor lasers," *Applied Physics Letters*, vol. 71, no. 1, pp. 19-21, 1997.
 [20] K. A. Williams, M. G. Thompson, and I. H. White, "Long-wavelength monolithic mode-locked diode lasers," *New Journal of Physics*, vol. 6, pp. 179-179, 2004/11/27 2004.
 [21] D. J. Derickson, et al., "Short pulse generation using multisegment mode-locked semiconductor lasers," *IEEE Journal of Quantum Electronics*, vol. 28, no. 10, pp. 2186-2202, 1992.